Proceedings of the 10th Brazilian Congress of Thermal Sciences and Engineering - ENCIT 2004
Braz. Soc. of Mechanical Sciences and Engineering - ABCM, Rio de Janeiro, Brazil, Nov. 29 - Dec. 03, 2004

AN ELEMENT-BASED FINITE VOLUME FORMULATION FOR SIMULATING TWO-PHASE IMMISCIBLE DISPLACEMENTS IN CORE SAMPLES

Fernando S. V. Hurtado
fernando@sinmec.ufsc.br

Clovis R. Maliska
maliska@sinmec.ufsc.br

Antonio F. C. da Silva
fabio@emc.ufsc.br

Jonas Cordazzo
jonas@sinmec.ufsc.br

Jaime Ambrus
jaime@sinmec.ufsc.br

Bruno A. Contessi
bruno@sinmec.ufsc.br

Federal University of Santa Catarina – UFSC
Computational Fluid Dynamics Laboratory – SINMEC
Department of Mechanical Engineering, 88040-900, Florianopolis, Santa Catarina, Brazil

Abstract. *This paper addresses the development of a numerical model for two-phase immiscible displacement in core samples, considering a two-dimensional representation of the flow. The final objective of this development is the application of such simulation tool on a parameter estimation methodology for determining relative permeability curves from experimental data collected in laboratory experiments. All possible influencing factors on the core-scale flow, such as rock heterogeneities, capillary pressure, gravity effects and fluid compressibility, are included in the model in order to cover a wide range of experimental scenarios and to deal with detailed porous media properties measurements now available from imaging methods. The Element-based Finite Volume Method (EbFVM) is used for discretizing the mass-conservation differential equations, whereas an accelerated version of the IMPES algorithm is proposed for solving them. Since EbFVM is a relatively novel method for simulating flow in porous media, in this paper is given special emphasis to the description of essential details in a systematic way, in order to provide a methodology basis for future developments in the reservoir simulation field.*

Keywords. *Element-based finite volume method, two-phase immiscible displacement, porous media, relative permeabilities.*

1. Introduction

Relative permeability curves are the key parameter for simulating multiphase flow in porous media. Since those curves contain fundamental information about the dynamic interaction of the fluid phases flowing in a specific porous media, they should be estimated on the basis of actual displacement experiments made on laboratory. On this type of experiments, typically, one of the fluid phases is injected into a core sample initially saturated with the other fluid phase, and the pressure drop and the displaced volume are measured during the transient process. The estimation of the relative permeability curves from these collected data is an ill-posed inverse problem, whose solution requires a theoretical model for the displacement process on the core sample. The Buckley-Leverett model was the basis for some of the earlier methods for solving that problem, but along the years several drawbacks of these methods have been reported in the literature. These deficiencies are mainly related with the oversimplification of the flow model, which neglects some phenomena that may have significant influence on the actual displacement process. In recent years, parameter estimation techniques are being increasingly applied for relative permeabilities determination, mostly because they allow employing a flow model as accurate as needed to represent all possible influencing factors on the core sample displacement. In this approach, functional representations of the relative permeability curves depending on a finite number of parameters are chosen, and then values of those parameters are estimated minimizing the differences between the experimental data and the numerical results obtained from the mathematical model.

The main purpose of this paper is the description of a two-dimensional numerical formulation developed for simulating two-phase displacement in core samples in a wide range of experimental scenarios. The long-term objective of this development is the integration of such simulation tool into a parameter estimation methodology for determining the most reliable possible relative permeability curves. Since hardly ever the core samples are homogeneous, the actual flow frequently deviates from the assumption of one-dimensionality that is widely considered in existent works related to that subject. Therefore, it was decided to extend the customary one-dimensional modeling to two dimensions. This

choice is justified by the fact that such two-dimensional formulation would be able to capture most of the heterogeneity-related phenomena, without increasing excessively the computational effort for solving the model equations, as certainly a three-dimensional model would do. Furthermore, in recent years considerably progress has been made in the application of imaging methods to accurately measure porous media intrinsic properties, i.e. porosity and absolute permeability, so the availability of required high-quality spatial distributions for those properties is assured.

The discretization of the flow model differential equations are carried out employing the Element-based Finite Volume Method (EbFVM). This approach follows the basic guidelines of the conventional finite volume method, namely the integration of differential equations over control volumes in a way that conservation is automatically enforced. However, a significant improvement in flexibility is introduced through the concept of element as the basic geometrical entity for discretization of the solution domain. As a matter of fact, all needed calculations are performed at element level and then the control-volume equations are assembled adding all element contributions in a way analogous to the assembling procedure commonly employed in the finite element method. Since the element-based finite volume method employing quadrangular element grids is a relatively novel approach for simulating flow in porous media, in this paper is given special emphasis to the description of essential details of the method in a systematic way. Furthermore, since the model equations for describing the multiphase flow at macroscopic level are essentially the same for displacements in core samples as well as in petroleum reservoirs, a parallel objective of this work is to develop a numerical framework for further developments in the reservoir simulation field. For solving the discretized equations was chosen a sequential solution algorithm similar to the standard IMPES (Implicit Pressure, Explicit Saturation) procedure, in which two modifications are introduced in order to accelerate its performance.

2. Mathematical model

The model employed is based on the standard macroscopic description of the flow of multiple immiscible fluid phases through porous media. Although the comparative significance of some physical factors over the flow can be different at reservoir-scale and at core-scale, the model equations for both scales are essentially the same when a macroscopic approach is employed. The main equations of the two-phase version of that model are briefly described in this section. The two fluid phases are designated as injected phase (I) and displaced phase (D), respectively.

The main components of the model are the mass-conservation differential equations for the two phases and the multiphase extension of Darcy's law. The former can be written as:

$$\phi\, \partial_t (\rho_F s_F) + \vec{\nabla} \cdot (\rho_F \vec{\mathbf{v}}_F) = 0; \qquad F = I, D \tag{1}$$

Here ρ_F, s_F and $\vec{\mathbf{v}}_F$ are the density, saturation and mean velocity vector of the given phase, respectively; ϕ is the porosity of the medium. The mean velocity of each phase is given by Darcy's law, which is usually extended to multiphase flow in the following way:

$$\vec{\mathbf{v}}_F = -\frac{K\, k_{rF}}{\mu_F} (\vec{\nabla} P_F - \rho_F \vec{\mathbf{g}}); \qquad F = I, D \tag{2}$$

where K is the absolute permeability of the porous medium, $\vec{\mathbf{g}}$ is the acceleration due to gravity, P_F is the phase pressure, μ_F is the phase viscosity, and k_{rF} is the phase relative permeability. Relative permeabilities account for the decrease on the capacity of one phase to flow due to reciprocal interference between the fluid phases.

The coupling between the preceding equations results from the volumetric restriction equation:

$$s_I + s_D = 1 \tag{3}$$

and the definition of capillary pressure:

$$P_C = P_D - P_I \tag{4}$$

Here, for convenience, that definition is used without any consideration about the wettability of the system. In addition to those equations, the dependency of densities, relative permeabilities and capillary pressure on state variables completes the coupling between the differential equations. Although from a theoretical point of view would be expected additional dependencies, in practice it is almost universally accepted that relative permeabilities and capillary pressure are only saturation functions:

$$k_{rF} = k_{rF}(s_I); \qquad F = I, D \tag{5}$$

$$P_C = P_C(s_I) \tag{6}$$

Additionally, the phase densities can be related to the corresponding phase pressures through a state equation. Assuming an isothermal flow, the state equations can be written in a generic way as

$$\rho_F = \rho_F(P_F); \qquad F = I, D \tag{7}$$

Boundary and initial conditions specification are required in order to complete the mathematical statement of a given displacement process. In this work, the vertical middle section of the core sample is taken as solution domain for the description of the displacement process, as depicted in Fig (1). On this two-dimensional domain, the upper and lower boundaries are impermeable because a sealant holder is always provided around the sample for laboratory experiments. At the sample inlet face, where one of the fluid phases is injected, it is assumed that there is no countercurrent flow of the other phase. This physical situation can be prescribed in the mathematical model as a zero velocity value for the displaced phase, along with either a velocity or a pressure boundary condition for the injected phase, depending on which one is controlled during the experiment.

The outlet face of the sample is usually subject to a constant pressure environment, so this known pressure value can be naturally imposed as a boundary condition for the displaced phase. The simultaneous flow of both phases through the outlet face can occur only if the phase pressures are continuous across that surface (Kulkarni et al., 1998). This condition is satisfied when capillary pressure decreases to zero, in any other situation only the non-wetting phase (the phase with higher pressure) will be able to flow out of the sample. This situation causes the accumulation of the wetting phase near the outlet face, until local saturation attains the value for which capillary pressure becomes zero (Bedrikovetsky et al., 1996). This phenomenon, commonly known as capillary end effect, will be modeled through the following boundary condition:

$$\begin{cases} (\vec{\mathbf{v}}_I \cdot \hat{\mathbf{n}})_{out} = 0 & \text{if } (P_C)_{out} > 0 \\ (\vec{\mathbf{v}}_D \cdot \hat{\mathbf{n}})_{out} = 0 & \text{if } (P_C)_{out} < 0 \\ (s_I)_{out} = s_I^{P_C=0} & \text{since the time when } (P_C)_{out} = 0 \end{cases} \tag{8}$$

where $\hat{\mathbf{n}}$ is the outward unit normal vector and $s_I^{P_C=0}$ is the saturation value that leads to a zero capillary pressure. Equation (8) is written according to the capillary pressure definition given by Eq. (4).

Equations (1) to (7) form a closed system that, along with the boundary and initial conditions, describes the spatial and temporal variation of the problem state-variables, namely phase pressures and saturations. Initial conditions should be provided for two of them, chosen as main variables in the solution algorithm. The injected phase saturation and the displaced phase pressure will be considered the main variables in this work.

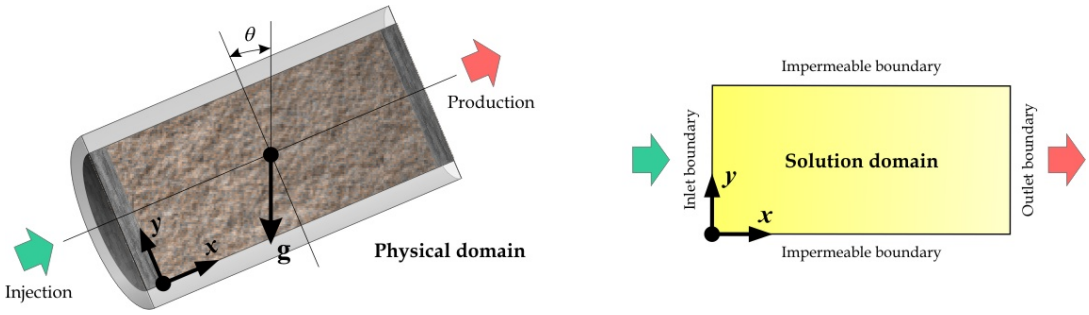

Figure 1. Two-dimensional domain considered in the flow model.

3. Element-based finite volume method fundamentals

For the application of the EbFVM, the solution domain must be broken up into much smaller sub-domains, called *elements*, which in this work are quadrilaterals. These entities are the basis for defining the geometry of the domain, as well as for storing the physical properties of the medium. The problem unknowns are calculated at points called *nodes*, located at every element corner. Around every node is built a *control volume*, formed by portions of the elements that share a common node. Every control volume is delimited by a certain number of *faces*, obtained joining the center of every neighboring element with the midpoint of its two sides sharing the node around which the control volume is built. As the surface integrals over the faces are commonly approximated by the midpoint rule (Raw, 1985), the face center points are commonly known as *integration points*. All these geometrical entities are depicted in Fig. (2).

As in any finite volume methodology, the conservation of physical quantities over every control volume is the essential premise of the EbFVM. Though, since the shape of the control volumes constructed following the previously described procedure can become extremely complex, a special approach is required in order to deal with the increased geometrical complexity. The strategy employed in the EbFVM, borrowed from the finite element technique, is the definition of a local coordinate system inside every element. Therefore, all needed calculations can be easily made based upon elements geometry, and then the conservation equations of every control volume can be simply assembled using the contributions coming from the neighboring elements.

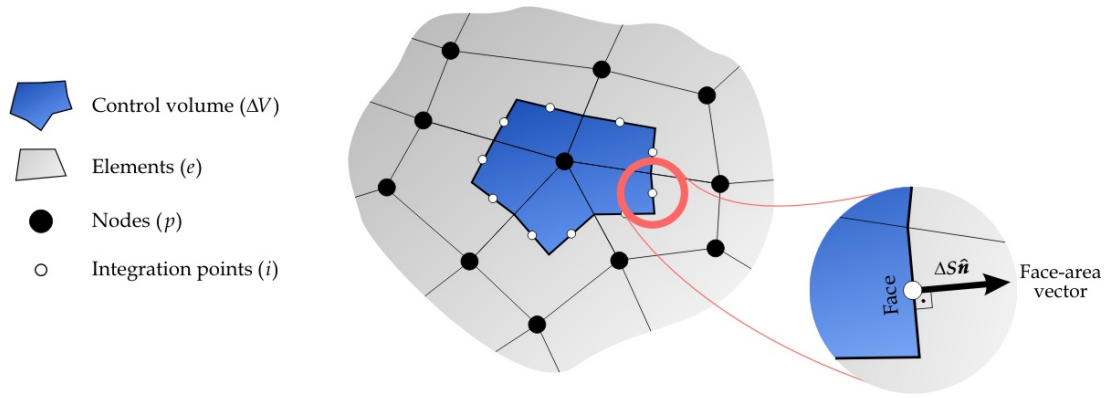

Figure 2. Main geometrical entities employed on the Element-based Finite Volume Method.

For quadrilateral elements, the coordinate transformation can be conveniently expressed employing the bilinear shape functions (Maliska, 2004):

$$\begin{cases} N_1(\xi,\eta) = \frac{1}{4}(1+\xi)(1+\eta) & N_2(\xi,\eta) = \frac{1}{4}(1-\xi)(1+\eta) \\ N_3(\xi,\eta) = \frac{1}{4}(1-\xi)(1-\eta) & N_4(\xi,\eta) = \frac{1}{4}(1+\xi)(1-\eta) \end{cases} \tag{9}$$

where ξ, η are the local coordinates inside an element. These coordinates can be related to the ones on a global coordinate system, employing the aforementioned shape functions in the following way:

$$\begin{cases} x(\xi,\eta) = \sum_{j=1}^{4} N_j(\xi,\eta)\, x_j \\ y(\xi,\eta) = \sum_{j=1}^{4} N_j(\xi,\eta)\, y_j \end{cases} \tag{10}$$

Here, x_j and y_j are the global coordinates at the j node of a given element, when a local node numbering, like the conventional one shown in Fig. (3a), is employed. No matter how distorted one element might be in terms of global coordinates, its representation in terms of local coordinates is always a regular square element, as shown in Fig. (3b). Inside this regular element, the variation of any state-variable can be approximated employing again the bilinear shape functions:

$$\Theta(\xi,\eta) \approx \sum_{j=1}^{4} N_j(\xi,\eta)\,\Theta_j = [N][\Theta]_e \tag{11}$$

where Θ is a generic state variable; for convenience, the summation was expressed alternatively as a product of a row vector $[N]$, containing the four shape functions, and a column vector $[\Theta]_e$, containing the four state-variable nodal values. This kind of notation will be employed also in subsequent equations.

It can be shown (Hurtado, 2004) that the gradient of a variable being approximated by Eq. (11) within the transformed element, may be expressed in matrix notation as

$$\vec{\nabla}\Theta \approx [J]^{-1}[D][\Theta]_e \tag{12}$$

Here, $[D]$ is an auxiliary matrix containing the partial derivatives of the shape functions ordered on the following way:

$$[D] = \begin{bmatrix} \partial_\xi N_1 & \partial_\xi N_2 & \partial_\xi N_3 & \partial_\xi N_4 \\ \partial_\eta N_1 & \partial_\eta N_2 & \partial_\eta N_3 & \partial_\eta N_4 \end{bmatrix} \tag{13}$$

and $[J]$ is the Jacobian matrix of the coordinate transformation, which can be easily obtained employing the derivatives matrix in the following way:

$$[J] = [D][Z]_e \tag{14}$$

where $[Z]_e$ is a 4×2 matrix containing the global coordinates x_j and y_j of the four nodes located at the corners of the given element, ordered in accordance with the local node numbering shown in Fig. (3).

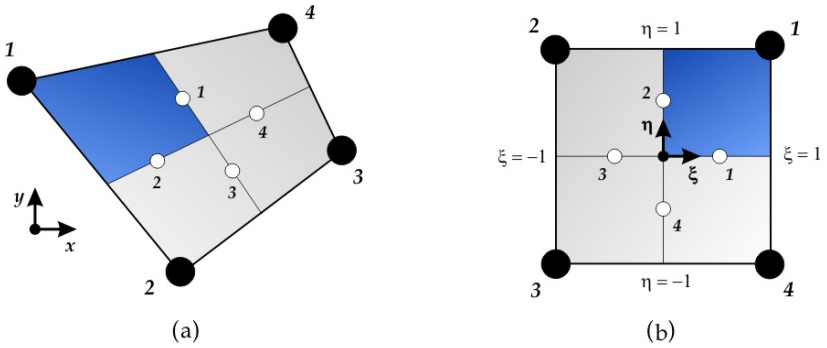

Figure 3. Isolated element in global and local coordinate system.

The oriented area-vectors of control volume faces are commonly needed during the discretizing process. These geometrical parameters can be obtained by means of the following expression (Hurtado, 2004):

$$(\hat{\mathbf{n}}\Delta S)_i = [R][J]_i^T[\Delta\sigma]_i \tag{15}$$

The subscript i identifies every integration point inside an element, as well as the face on which it is on, according to the conventional numbering shown in Fig. (3). In Eq. (15), $[\Delta\sigma]_i$ is a row vector that takes the values $[1\ 0]$, $[0\ 1]$, $[-1\ 0]$, and $[0\ -1]$ for the faces 1, 2, 3, and 4, respectively. In addition, $[R]$ is a 90º clockwise rotation matrix, given by

$$[R] = \begin{bmatrix} 0 & 1 \\ -1 & 0 \end{bmatrix} \tag{16}$$

4. Discretization process

4.1. The pressure equation

In order to solve numerically the multiphase flow equations, several options exist for choosing the main variables and time-related approximations that, regardless of the type of spatial discretization considered, lead to different solution algorithms. In this work was chosen an IMPES-type sequential approach, where the main variables are the displaced phase pressure and the injected phase saturation. Each one of these variables needs an evolution equation in order to advance them in time throughout the solution process. In this section is deduced the discrete equation for the pressure, employing the EbFVM for discretizing the differential equations in space.

The integration of the mass-conservation differential equations, Eq. (1), over a generic control volume like the one depicted in Fig. (2), leads to

$$\int_{\Delta V} \partial_t(\rho_F s_F)\,\phi\, dV + \int_{\Sigma\Delta S} \rho_F \vec{\mathbf{v}}_F \cdot \hat{\mathbf{n}}\, dS = 0; \qquad F = I, D \tag{17}$$

The divergence theorem has been employed in order to transform the second volume integral into a surface integral over the control volume boundary. Approximating the integrals by means of the midpoint rule (Raw, 1985) and the time derivative by a backward finite differences expression, the following discrete analog of Eq. (17) is obtained:

$$(\rho_F s_F - \rho_F^o s_F^o)_p \frac{\phi_p \Delta V_p}{\Delta t} + \sum_i (\rho_F \vec{\mathbf{v}}_F \cdot \hat{\mathbf{n}}\,\Delta S)_i = 0; \qquad F = I, D \tag{18}$$

Along this paper, the subscripts outside parentheses will denote the location where the inside terms are evaluated; the subscript p designates the nodes, whereas the subscript i designates the integration points. Furthermore, the superscript o denotes variables from the preceding time level.

After substitution of Eq. (2) into Eq. (18), the following equation is obtained:

$$\frac{(\rho_F s_F - \rho_F^o s_F^o)_p}{\Delta t}\phi_p \Delta V_p - \sum_i \left[\rho_F \lambda_F (\vec{\nabla} P_F - \rho_F \vec{\mathbf{g}}) \cdot \hat{\mathbf{n}}\Delta S\right]_i = 0; \qquad F = I, D \tag{19}$$

where λ_F stands for the phase mobility, which is defined as

$$\lambda_F = \frac{K k_{rF}}{\mu_F}; \qquad F = I, D \tag{20}$$

Since Eq. (18) is highly non-linear, some decisions should be made in order to deal with its non-linearities. In this work is used an IMPES-type sequential solution algorithm, so all saturation-dependent terms except the one coming from the transient term will be treated explicitly, that is, they will be evaluated with saturation values from the previous time level. As a result, the only non-linearities remaining in Eq. (19) would be those coming from products of variables involving density. With the aim of linearizing the terms related to mass-fluxes across the control volume faces, it was decided to employ explicit densities in those terms. On the other hand, the density-saturation product on the transient term was linearized by means of the following truncated Taylor expansion:

$$\rho_F s_F \approx \rho_F^o s_F + \rho_F s_F^o - \rho_F^o s_F^o; \qquad F = I, D \tag{21}$$

As the density might be by itself a non-linear function of the phase pressure, in that case should be necessary to linearize the functional relationship, Eq. (7). Regardless of the linearization nature, that approximation can be written as

$$\rho_F \approx a_{F1} P_F + a_{F2}; \qquad F = I, D \tag{22}$$

After introducing the preceding approximations on equation (19) and eliminating the current-time saturation variables by means of Eq. (3), the phase pressures are the only state-variables remaining on the resulting equation. It can be further simplified expressing one of the phase pressures in function of the other and explicit values of capillary pressure. The resulting equation is the pressure equation for the IMPES solution algorithm, which can be conveniently arranged in the following way:

$$\sum_i b_{p,i}^P (\vec{\nabla} P_D \cdot \hat{\mathbf{n}} \Delta S)_i + c_p^P (P_D)_p = \sum_i d_{p,i}^P (\vec{\nabla} P_C^o \cdot \hat{\mathbf{n}} \Delta S)_i + \sum_i e_{p,i}^P (\vec{\mathbf{g}} \cdot \hat{\mathbf{n}} \Delta S)_i + f_p^P \tag{23}$$

where the coefficients appearing on Eq. (23) are defined on the first column of Tab. (1).

The calculation of the integration points-related contributions on the summation terms of Eq. (23) can be easily made employing the local coordinate system. Furthermore, in order to facilitate the equation assembling process, the contributions over the balance equations of the four control volumes overlapping a given element can be arranged in matrix form. For instance, the matrix analog of the summation terms of Eq. (23) within an element may be written as (Hurtado, 2004):

$$\left[\sum_i b_{p,i}^P (\vec{\nabla} P_D \cdot \hat{\mathbf{n}} \Delta S)_i \right]_e = \begin{bmatrix} b_{1,1}^P [B]_1 - b_{1,2}^P [B]_2 \\ b_{2,2}^P [B]_2 - b_{2,3}^P [B]_3 \\ b_{3,3}^P [B]_3 - b_{3,4}^P [B]_4 \\ b_{4,4}^P [B]_4 - b_{4,1}^P [B]_1 \end{bmatrix} \begin{bmatrix} P_{D1} \\ P_{D2} \\ P_{D3} \\ P_{D4} \end{bmatrix} \equiv [A^*]_e^P [P_D]_e \tag{24}$$

$$\left[\sum_i d_{p,i}^P (\vec{\nabla} P_C^o \cdot \hat{\mathbf{n}} \Delta S)_i + \sum_i e_{p,i}^P (\vec{\mathbf{g}} \cdot \hat{\mathbf{n}} \Delta S)_i \right]_e = \begin{bmatrix} d_{1,1}^P [B]_1 - d_{1,2}^P [B]_2 \\ d_{2,2}^P [B]_2 - d_{2,3}^P [B]_3 \\ d_{3,3}^P [B]_3 - d_{3,4}^P [B]_4 \\ d_{4,4}^P [B]_4 - d_{4,1}^P [B]_1 \end{bmatrix} \begin{bmatrix} P_{C1}^o \\ P_{C2}^o \\ P_{C3}^o \\ P_{C4}^o \end{bmatrix} + \begin{bmatrix} e_{1,1}^P G_1 - e_{1,2}^P G_2 \\ e_{2,2}^P G_2 - e_{2,3}^P G_3 \\ e_{3,3}^P G_3 - e_{3,4}^P G_4 \\ e_{4,4}^P G_4 - e_{4,1}^P G_1 \end{bmatrix} \equiv [F^*]_e^P \tag{25}$$

Here, the row vector $[B]_i$ stands for the element geometry-dependent part of the term $(\vec{\nabla} P \cdot \hat{\mathbf{n}} \Delta S)_i$. This row vector is given by the expression:

$$[B]_i = \left([R][J]_i^T [\Delta\sigma]_i \right)^T [J]_i^{-1} [D]_i \tag{26}$$

which is easily obtained combining Eq. (12) and Eq. (15). In addition, G_i is a gravity-dependent parameter defined by

$$G_i \equiv (\vec{\mathbf{g}} \cdot \hat{\mathbf{n}} \Delta S)_i = -g [\sin\theta \quad \cos\theta] [R][J]_i^T [\Delta\sigma]_i \tag{27}$$

where the θ is the inclination angle of gravity vector as depicted in Fig. (1). It is important to note that the node and integration point numbering in Eq. (24) and (25) is referred to the conventional numbering showed in Fig (3).

Equations (24) and (25) can be taken as definition equations for the pressure-equation element matrix $[A^*]_e^P$ and element column vector $[F^*]_e^P$. An assembling procedure, similar to the one commonly employed in the finite element methodology (Zienkiewicz, 1989), can be used to gather the information contained in these element matrices and vectors in order to obtain a global matrix and a global vector representing all control-volume equations. This matrix assembling procedure, illustrated in Fig. (4) for a three-element grid, consists in the addition of each element matrix cell-value to a given cell-value on the global matrix, whose location is univocally specified by the global numbering of

nodes. This information is commonly stored in a table, commonly known as connectivity table, where every row contains the global identification numbers of a given element nodes, as depicted in Fig. (4b). The described assembling procedure, performed employing the element matrices $[A^*]_e^P$ and column vectors $[F^*]_e^P$, is totally equivalent to adding all contributions of the surrounding elements on the summation terms of Eq. (23), simultaneously for all control volumes. Symbolically, the global matrix and column vector for the pressure equation will be given by

$$[A^*]^P = \mathop{\mathbf{M}}_{e=1}^{N_{elm}} [A^*]_e^P \tag{28}$$

$$[F^*]^P = \mathop{\mathbf{M}}_{e=1}^{N_{elm}} [F^*]_e^P \tag{29}$$

where **M** is an operator representing the assembling procedure depicted in Fig. (4), and N_{elm} is the total number of elements in the grid. Since in the element matrix and column vector definition were only included terms related to integration points, the matrix $[A^*]^P$ and the vector $[F^*]^P$ still do not represent entirely the system of equations for the pressure. In order to complete the equations, the node-related terms of Eq. (23) should be added to the diagonal cell-values of the matrix $[A^*]^P$ and to the corresponding elements of the column vector $[F^*]^P$ in the following way:

$$A_{p,p}^P = A_{p,p}^{*P} + c_p^P \tag{30}$$

$$F_p^P = F_p^{*P} + f_p^P \tag{31}$$

Here p is the control volume identification number, in this case the same as the global node number. After performing these operations for all control volumes, the resulting global matrix and column vector contain the coefficients and independent terms, respectively, of the displaced phase pressure system of equations:

$$[A]^P[P_D] = [F]^P \tag{32}$$

Before solving this system of equations, the respective boundary conditions of the problem should be inserted into the equations corresponding to boundary-adjacent control volumes. Additional details about this procedure can be found elsewhere (Hurtado, 2004).

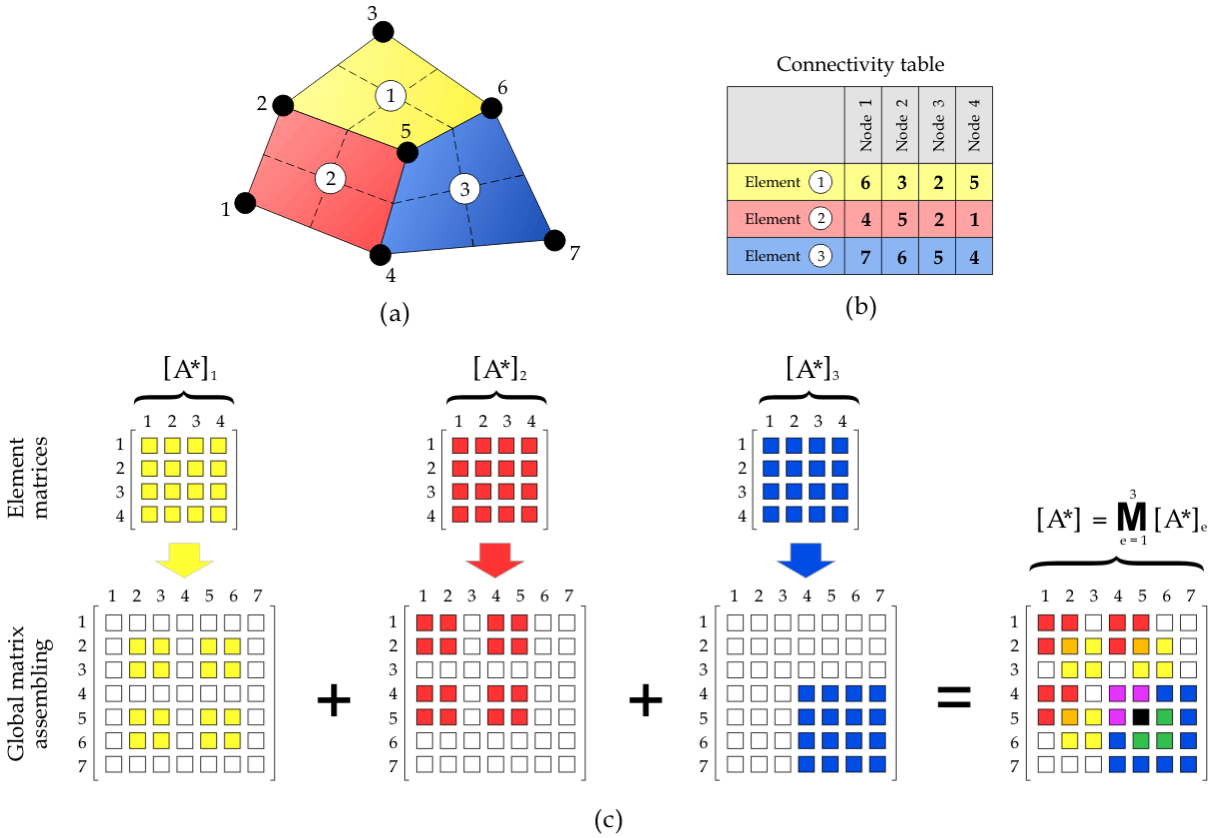

Figure 4. Schematic representation of the matrix assembling procedure for a three-element grid.

Table 1. Definition of coefficients for pressure and saturation equations

Pressure equation coefficients	Saturation equation coefficients
$b^P_{p,i} = -\left[\dfrac{(\rho^o_I\lambda^o_I)_i}{(\rho^o_I)_p} + \dfrac{(\rho^o_D\lambda^o_D)_i}{(\rho^o_D)_p}\right]$	$b^s_i = \left(\rho^o_D F^o \lambda^o_D \dfrac{dP_C}{ds_I}\bigg\vert^o\right)_i$
$c^P_p = \dfrac{\phi_p \Delta V_p}{\Delta t}\left(\dfrac{a_{I1}s^o_I}{\rho^o_I} + \dfrac{a_{D1}s^o_D}{\rho^o_D}\right)_p$	$c^s_p = (\rho_I)_p \dfrac{\phi_p \Delta V_p}{\Delta t}$
$d^P_{p,i} = -\left[\dfrac{(\rho^o_I\lambda^o_I)_i}{(\rho^o_I)_p}\right]$	$d^s_i = -(\rho^o_I F^o)_i$
$e^P_{p,i} = -\left[\dfrac{(\rho^o_I)^2_i(\lambda^o_I)_i}{(\rho^o_I)_p} + \dfrac{(\rho^o_D)^2_i(\lambda^o_D)_i}{(\rho^o_D)_p}\right]$	$e^s_i = -[\rho^o_I F^o \lambda^o_D(\rho^o_I - \rho^o_D)]_i$
$f^P_p = \dfrac{\phi_p \Delta V_p}{\Delta t}\left(\dfrac{a_{I1}s^o_I}{\rho^o_I}P^o_C - \dfrac{a_{I2}s^o_I}{\rho^o_I} - \dfrac{a_{D2}s^o_D}{\rho^o_D} + 1\right)_p$	$f^s_p = (\rho^o_I s^o_I)_p \dfrac{\phi_p \Delta V_p}{\Delta t}$

4.2 The saturation equation

Following the standard IMPES solution algorithm, the injected phase mass-conservation discretized equation, Eq. (19) written for that phase, could be used to calculate directly all nodal values of the injected phase saturation after the pressure system of equations being solved. Although this is one of the simplest approaches used to solve the multiphase equations, it suffers from a severe stability restriction on the timestep, caused by the explicit evaluation of saturation dependent quantities, i.e. mobilities and capillary pressure. Since this limitation may cause the numerical simulations become excessively time-consuming, especially when the capillary pressure influence is significant (Mattax and Dalton, 1990), a slightly different approach was used in this work. For obtaining a discrete equation for the evolution of the injected phase saturation was used the so-called Buckley-Leverett form of the saturation equation (Peaceman, 1977):

$$\phi\,\partial_t(\rho_I s_I) + \vec{\nabla}\cdot(\rho_I F \vec{\mathbf{v}}_T) + \vec{\nabla}\cdot(\rho_I \lambda_D F \vec{\nabla} P_C) + \vec{\nabla}\cdot[\rho_I \lambda_D F(\rho_I - \rho_D)\,\vec{\mathbf{g}}] = 0 \tag{33}$$

where $\vec{\mathbf{v}}_T$ is the total velocity vector, defined as

$$\vec{\mathbf{v}}_T = \vec{\mathbf{v}}_I + \vec{\mathbf{v}}_D \tag{34}$$

and F is the fractional flux function, which is exclusively dependent on saturation, which is defined as

$$F = \frac{\lambda_I}{\lambda_I + \lambda_D} \tag{35}$$

Equation (33) is totally equivalent to the injected-phase version of Eq. (1), but it is more suitable for numerical purposes because of some special features. In the present formulation, using that equation allows to speed-up the performance of the solution algorithm in two different ways. First, the timestep stability limitation can be partially overcome by means of a semi-implicit treatment of the capillary pressure term, as proposed at first by Spillette et al., (1973). This kind of treatment does not introduce any inconsistency because the total velocity calculated for solving Eq. (33) is the same whether the capillary pressure term in the pressure equation is evaluated explicitly or implicitly (Peaceman, 1977). Besides, since total velocity usually evolves slower than pressure, the frequency of pressure actualization could be reduced, leading to a faster performance of the sequential solution algorithm. This feature will be discussed in the next section.

The capillary pressure semi-implicit treatment comes from the following approximation for the capillary pressure gradient:

$$\vec{\nabla} P_C \approx \frac{dP_C}{ds_I}\bigg\vert^o \vec{\nabla} s_I \tag{36}$$

where, in order to linearize it, the capillary pressure derivative is evaluated with previous-timestep saturation values. After introducing that approximation into Eq. (33), this equation can be integrated over a control volume following the same procedure described for obtaining the discrete pressure equation in the previous section. The resulting discrete equation can be written as:

$$\sum_i b_i^s (\vec{\nabla} s_I \cdot \hat{\mathbf{n}} \Delta S)_i + c_p^s (s_I)_p = \sum_i d_i^s (\vec{\mathbf{v}}_T \cdot \hat{\mathbf{n}} \Delta S)_i + \sum_i e_i^s (\vec{\mathbf{g}} \cdot \hat{\mathbf{n}} \Delta S)_i + f_p^s \tag{37}$$

The coefficients for this equation are detailed in the second column of Tab. (1). As Eq. (37) has similar form to the pressure equation, Eq. (23), the assembling procedure already described can be used to obtain a system of equations for the saturation. In this case, the element matrix and column vector containing the integration point-related contributions to Eq. (37) result in

$$[A^*]_e^s = \begin{bmatrix} b_1^s[B]_1 - b_2^s[B]_2 \\ b_2^s[B]_2 - b_3^s[B]_3 \\ b_3^s[B]_3 - b_4^s[B]_4 \\ b_4^s[B]_4 - b_1^s[B]_1 \end{bmatrix} \tag{38}$$

$$[F^*]_e^s = \begin{bmatrix} d_1^s q_{T1} - d_2^s q_{T2} \\ d_2^s q_{T2} - d_3^s q_{T3} \\ d_3^s q_{T3} - d_4^s q_{T4} \\ d_4^s q_{T4} - d_1^s q_{T1} \end{bmatrix} + \begin{bmatrix} e_1^s G_1 - e_2^s G_2 \\ e_2^s G_2 - e_3^s G_3 \\ e_3^s G_3 - e_4^s G_4 \\ e_4^s G_4 - e_1^s G_1 \end{bmatrix} \tag{39}$$

where q_{Ti} is the volumetric flow-rate across a control volume face, given by

$$q_{Ti} = (\vec{\mathbf{v}}_T \cdot \hat{\mathbf{n}} \Delta S)_i \tag{40}$$

Finally, after assembling the element matrices and column vectors and adding the terms of Eq. (37) related to the transient term, the system of equations for the injected phase saturation results in

$$[A]^s [s_I] = [F]^s \tag{41}$$

5 Solution algorithm

Although the semi-implicit treatment of capillary pressure considered here actually reduces the stability restriction, the limitation caused by explicit evaluation of mobilities still subsists. It is well known that the standard IMPES algorithm can become markedly slow for practical applications because of this stability restriction, which prevents the use of larger simulation timesteps. In fact, this timestep limitation is more closely related to the saturation equation than to the pressure equation. As pointed out by Chippada (1997), the pressure equation could be solved with larger timesteps without affecting the algorithm stability. Thus, a modified version of the IMPES procedure can be devised, where different timesteps are used, one satisfying Eq. (42) for the saturation equation, and a multiple of the former for the pressure equation. This modification results in a great computation-time saving because of the reduction on the number of times that pressure equation must be solved throughout a simulation. It is remarkable the fact that, depending on the timestep ratio used, the quality of numerical simulations is seldom degraded, as will be shown in the next section.

The main steps of the solution algorithm employed can be summarized as follows:

1. Initialize the discrete fields according to the initial conditions.
2. Solve the linear system of equations for the displaced phase pressure, Eq. (32).
3. Compute the phase velocities at integration points by means of Darcy law, and then evaluate the total velocity by means of Eq. (34).
4. Solve the linear system of equations for the injected phase saturation, Eq. (41), a fixed number of times with the same total velocity field.
5. Advance in time and return to step 2.

It is noteworthy the fact that streamlines-based methods for reservoir simulation (Thiele et al., 1996) achieve faster performances than conventional methods because of a solution algorithm that shares some characteristics with the one outlined above. In those methods, streamlines are obtained with a calculated velocity field, and then saturations are advanced in time solving 1-D displacement equations along the streamlines, either analytically or numerically. If necessary, velocity field and streamlines are recomputed periodically. In the proposed sequential algorithm, it is no needed to compute streamlines but total velocity field is updated only after a certain number of saturation iterations.

Another feature of the proposed numerical formulation that can lead to increased efficiency in computational performance is the manner in which element matrices are constructed. Every integration point-related contribution in those matrices was always expressed as a product of a geometry-dependent row vector and a flow-dependent coefficient. The former can be computed only once, before starting the iterative solution process; consequently, at every iteration only must be updated the flow-dependent part. This approach resembles the conventional finite volume method

approach where transmissibilities, a geometry-dependent parameter, are calculated once, remaining only mobilities to be updated during the iterative process. In the proposed formulation, the situation is certainly more complex because of the generality of the element-based approach.

6. Aplication examples

In this section will be presented some application examples with two main objectives: to compare solutions obtained using both structured and unstructured grids and to evaluate the performance of the accelerated version of the IMPES algorithm. In all examples the solution domain is the vertical middle section of a core sample whose dimensions are showed in Fig. (5a). This domain was discretized considering a 3600-element Cartesian grid and a 3582-element unstructured grid; details of topology of such grids are depicted in Fig. (5b) and Fig. (5c), respectively. An imbibition displacement was simulated where the injected phase is water and the displaced phase is oil. A constant water flow-rate of $Q_I = 0.5\,cm^3/min$ is injected into the sample, which is initially at irreducible water condition, $s_I^{\inf} = 0.1$. Moreover, the residual oil saturation value is $s_D^{\inf} = 0.2$, while water viscosity is $\mu_I = 0.001\,Pa \cdot s$ and oil viscosity is $\mu_D = 0.04\,Pa \cdot s$. The spatial variation of absolute permeability and porosity used are shown in Fig. (6a) and (6b), respectively. Those maps were obtained by nuclear magnetic resonance imaging methods, by Zuluaga et al. (2002). The relative permeability curves considered, typical of an imbibition displacement, are represented in Fig. (6c), while the non-dimensional capillary pressure curve is shown in Fig. (6d). The capillary pressure values were non-dimensionalized by means of the initial pressure drop across the sample.

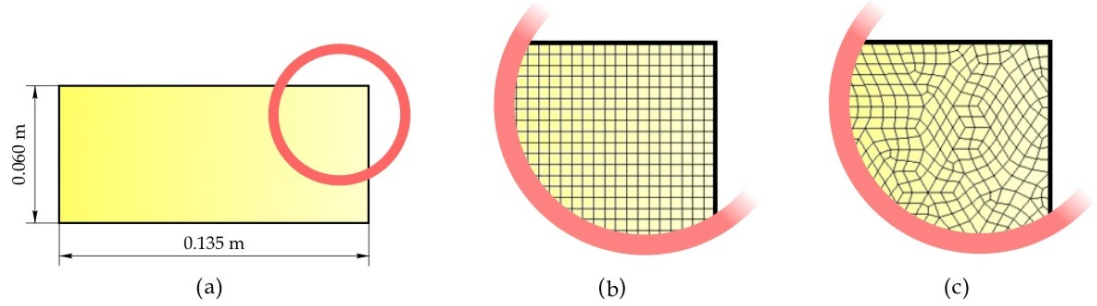

Figure 5. Solution-domain dimensions and details of the employed grids

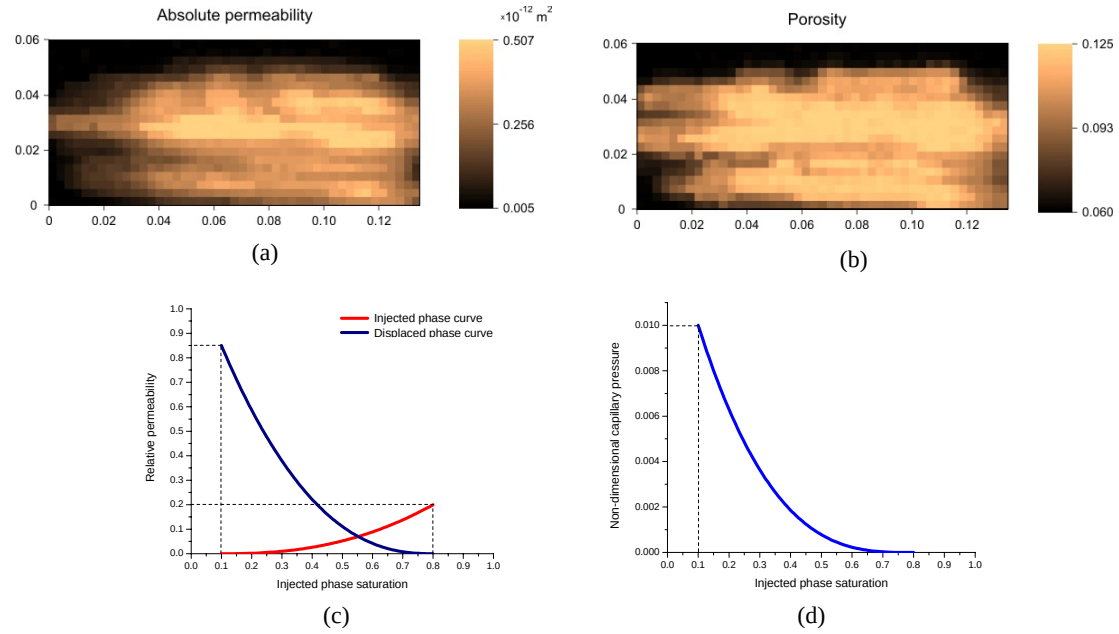

Figure 6. Absolute permeability and porosity distribution maps; relative permeability and non-dimensional capillary pressure curves

Figure (7) shows the comparison between simulations obtained with the Cartesian and the unstructured grid, for three selected times. The saturation distributions show the markedly influence of medium heterogeneity over the displacement. Regardless of the different grid topology, the distributions obtained are almost identical, at least in the two earlier times, before the front arrives in the outlet boundary. After the arrival, it is more evident some minor

discrepancy between the saturation distributions. In this later time is clearly observed the presence of the capillary end-effect as a region of high saturation gradient. In this case water is the wetting phase, and it can only pass through the outlet boundary if saturation attains the value that leads to a zero capillary pressure. Hence, this phase accumulates near the outlet face until that condition be satisfied, generating the end effect phenomenon.

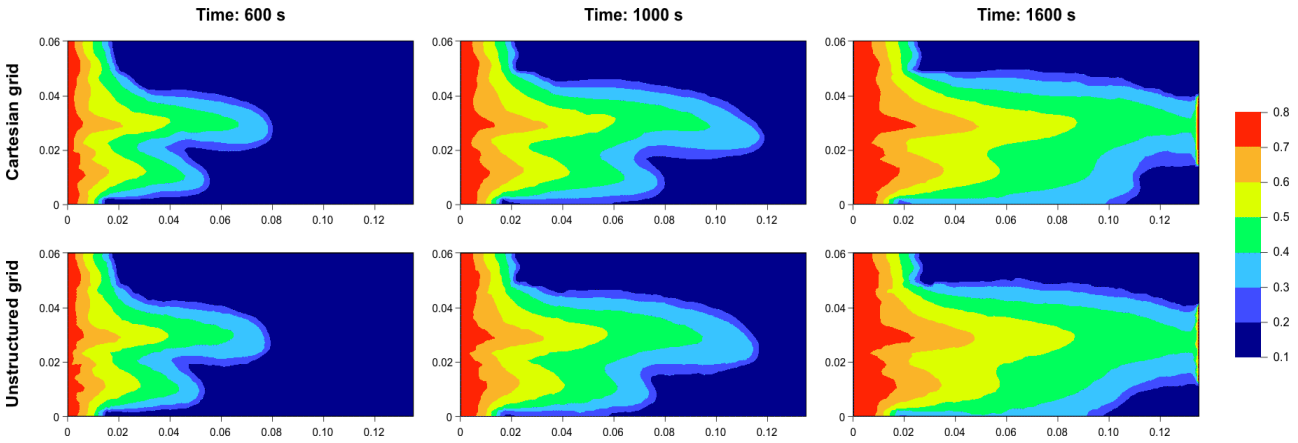

Figure 7. Comparison of saturation distributions at three selected times

In order to evaluate the performance of the proposed modified version of the IMPES sequential algorithm, three new simulations on the Cartesian grid were obtained varying the ratio between timesteps on pressure and saturation equations. This timestep ratio is equivalent to the number of times that saturation equation is solved until pressure equation is solved again for updating the total velocity field. In Fig. (8) are represented the saturation distributions for two selected times and three timestep ratios. The reference solution is the one corresponding to a time step ratio equal to one, which is equivalent to a conventional-IMPES solution. As can be observed in Fig. (8), the increasing of timestep ratio does not imply a significant reduction in quality of the simulations. As a matter of fact, the simulations are nearly identical, being perhaps the differences among them less important than the inherent discretization error. A more accurate comparison can be achieved through the superimposition of saturation profiles as performed in Fig. (9). Three equally-spaced horizontal cut-lines were considered in the solution domain, as is shown in Fig. (9a), for representing saturation profiles along each one of them. The comparison of the profiles corresponding to different timestep ratios shows even more categorically the proximity of the numerical solutions. Even more remarkable is the reduction of computation time obtained in this case: 38% and 65.3% for timestep ratio values of 2 and 5, respectively. In situations where capillary pressure influence is negligible or where sample heterogeneity-level is minor, were obtained even larger computation-time savings. Although it is possible to use larger values of the timestep ratio, further computation-time reductions are not significant, at least in most of the cases tested.

7. Conclusions

This paper has presented a two-dimensional numerical model for two-phase immiscible displacements in core samples, grounded in the Element-based Finite Volume Method (EbFVM). Since the long-term objective of this development is the implementation of a simulation tool into a parameter estimation methodology for obtaining relative permeability curves, it was attempted to include all possible physical influencing factors on the displacement process at core-scale. Fundamental steps of the differential equation discretization process was described in detail, in order to systematize the application of the EbFVM, a slightly novel method in the field of porous media flow simulation. For solving the discretized equations was described a sequential solution algorithm, that can be considered an accelerated version of the conventional IMPES procedure. The imbibition displacement process on a highly heterogeneous core sample was simulated for testing the performance of the proposed numerical model. Simulations on both a Cartesian and an unstructured grid were obtained, being the results quite similar. This evidences that the presented numerical formulation can be used with any type of quadrilateral grids. Comparisons were also made employing various timestep ratios in order to reduce the computational time needed to obtain a given simulation. As expected, larger timestep ratios led to high reductions in computational time. It was verified that those time reductions do not imply a significant decrease in the quality of numerical simulations.

8. Acknowledgements

This work was supported by Agência Nacional do Petroleo (ANP), through PRH 09 - Programa de Formação de Recursos Humanos em Petróleo e Gás. We gratefully acknowledge also financial support and cooperation of Petróleo Brasileiro S. A. (Petrobras).

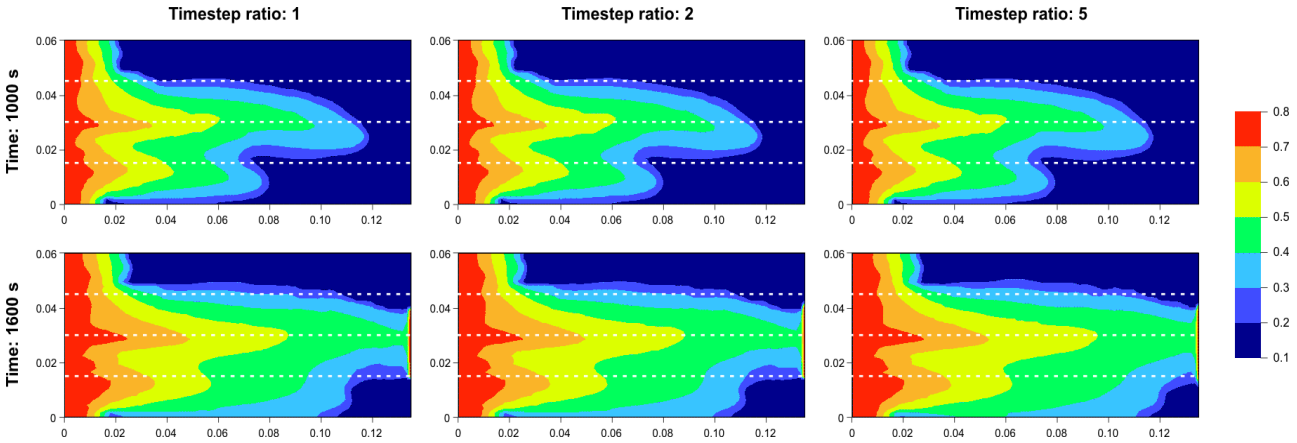

Figure 8. Comparison of saturation distributions obtained with three different timestep ratios

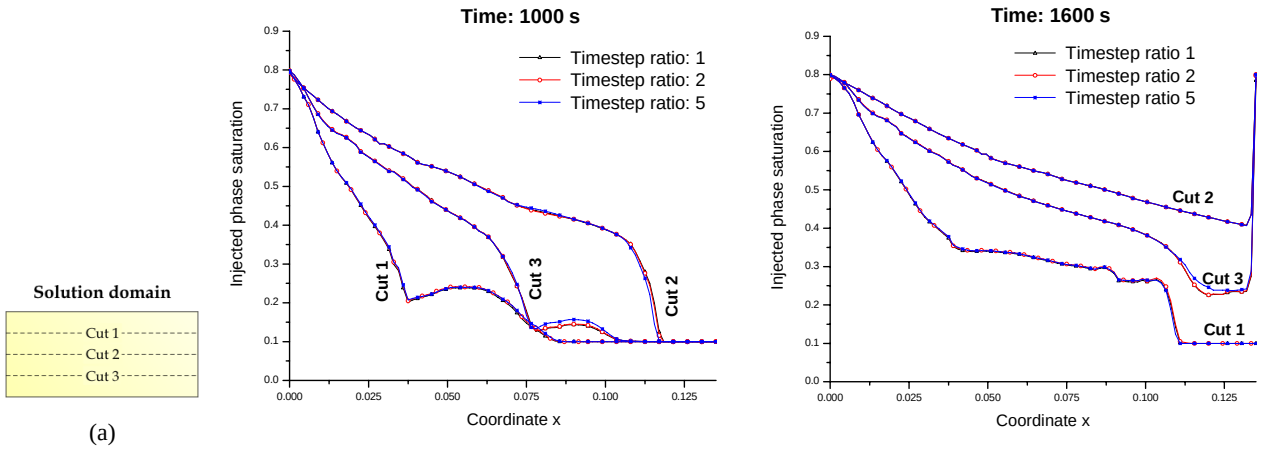

(a) (b) (c)

Figure 9. Comparison of saturation profiles at three horizontal cut-lines and two selected times

9. References

Bedrikovetsky, P., Rodrigues, J. R. P. and Brito, P. R. F., 1996, "Analytical Model for the Waterflood Honouring Capillary Pressure (With Application to Laboratory Studies)", Paper SPE 36130.

Chipadda, S., 1997, "A Procedure for Accelerating IMPES/SEQ", 7th Annual Industrial Affiliates Meeting, Center for Subsurface Modeling, University of Texas, United States of America.

Hurtado, F. S. V., 2004, "Uma Formulação de Volumes Finitos Baseada em Elementos para a Simulação do Deslocamento Bifásico Imiscível em Meios Porosos", Dissertação de Mestrado, Universidade Federal de Santa Catarina, Florianópolis, Brasil.

Kulkarni, R., Watson, A. T., Nordtvedt, J. E., and Sylte, A., 1998, "Two-phase Flow in Porous Media: Property Identification and Model Validation", AIChE Journal, Vol. 44, No. 11, pp. 2337-2350.

Maliska, C. R., 2004, "Transferência de Calor e Mecânica dos Fluidos Computacional", 2ª Edição Revista e Ampliada, Livros Técnicos e Científicos Editora S. A., Rio de Janeiro, Brasil.

Mattax, C. C. and Dalton, R. L., 1990, "Reservoir Simulation", SPE Monograph Series, Volume 13, Society of Petroleum Engineers.

Peaceman, D. W., 1977, "Fundamentals of Numerical Reservoir Simulations", Developments in Petroleum Science, Volume 6, Elsevier Scientific Publishing Company.

Raw, M. J., 1985, "A New Control-volume-based Finite Element Procedure for the Numerical Solution of the Fluid Flow and Scalar Transport Equations", Ph. D. Thesis, University of Waterloo, Ontario, Canada.

Spillette, A. G., Hillestad, J. G., and Stone, H. L., 1973, "A High-stability Sequential Solution Approach to Reservoir Simulation", Paper SPE 4542.

Thiele, M. R., Batycky, R. P., Blunt, M. J. and Orr, F. M., 1996, "Simulating Flow in Heterogeneous Systems Using Streamtubes and Streamlines", SPE Reservoir Engineering, February 1996, pp. 5-12.

Zienkiewicz, O. C., 1989, "The Finite Element Method", Volume 1, Fourth Edition, McGraw-Hill International Editions.

Zuluaga, E. Majors, P. D., and Peters, E. J., 2002, "A Simulation Approach to Validate Petrophysical Data from NMR Imaging", SPE Journal, March 2002, pp. 35-39.